

Dynamical conductivity in multiply-degenerate point-nodal semimetal CoSi

Tetsuro Habe

Department of Applied Physics, Hokkaido University, Sapporo, Hokkaido 060-0808, Japan

(Dated: March 13, 2019)

We investigate the dynamical conductivity in multiply-degenerate point-nodal semimetal CoSi by using first-principles band calculation and linear response theory. The semimetal holds point nodes in the electronic band structure. Around the nodes, electronic states are represented as multi-fold chiral fermions. We find some characteristic structures associated with the electronic structure in the spectrum of dynamical conductivity as a function of the photon frequency. Especially in the low-frequency region, a dip structure and a flat-top peak are ascribable to the electronic property of the chiral fermion and the effect of spin-orbit coupling, respectively. The numerical result can provide the relation between the profile of dynamical conductivity and electronic states in the point-nodal semimetal.

I. INTRODUCTION

Topological nodal semimetals have attracted much attention in condensed matter physics due to the electronic structure. In point-nodal semimetals, the conduction and valence bands touch each other at points, called nodes, in the Brillouin zone.¹ Dirac and Weyl semimetals are the first generation of topological point-nodal semimetals.²⁻⁶ The electronic states around the nodes are described by Dirac equation in high-energy physics and show fascinating electronic properties unlike conventional metals. Recently, a novel type of point-nodal semimetals has been proposed theoretically and predicted to have multiply degenerate electronic states, so-called multi-fold chiral fermion, which can not be described by Dirac equation at the nodes.⁷⁻⁹ Such topological nodal semimetals have been expected to provide novel electronic property beyond Dirac fermions.

CoSi is a strong candidate of the novel topological semimetals according to the first principles band calculation.^{8,10,11} Angle-resolved photoemission spectroscopy (ARPES) is one of the experimental techniques for determining such topological semimetallic electronic structure. Recently, a few groups have reported the band structure of CoSi by using ARPES and shown nodes and topological surface states, one of the characteristic feature of topological materials.^{12,13} However, there is a restriction in the visible electronic energy for ARPES because it is able to reveal the dispersion relation up to the Fermi level. In high quality single crystals of semimetal, the Fermi level is pinned at the charge neutral point, and it is slightly below one of the nodes in CoSi. Therefore, the other measurement is necessary for revealing the electronic property of excited electronic states.

In this paper, we theoretically investigate the dynamical conductivity of CoSi by combining first-principles calculation and linear response theory. The dynamical conductivity is associated with the inter-band excitation between the conduction and valence bands, and thus it is able to provide the information of electronic bands above the Fermi level. In Ref. 14, it is shown that the numerical result by using the first-principles calculation for a topological semimetal has a good agrees with the experimen-

tal measurement¹⁵ even in a high photon-energy region. We discuss the relation between the spectrum of dynamical conductivity and the electronic band structure, and find some characteristics reflecting the electronic structure of the topological semimetals.

II. FIRST-PRINCIPLES BAND STRUCTURE

We calculate the electronic band structure of CoSi by using quantum ESPRESSO, a first-principles calculation code,¹⁶ and show it in Fig. 1 (b). The cubic unit cell and Brillouin zone are schematically depicted in Fig. 1 (a). The lattice constant and the atomic position are computed within the same code by relaxing the lattice to the stable structure. Then, the lattice constant is estimated to be 4.432Å and the atomic position is given in Table II. The crystal structure is classified into $P2_13$ with factors of $x_{\text{Co}} = 0.144$ and $x_{\text{Se}} = 0.843$ for Co and Se, respectively. We apply a projector augmented wave method to the first-principles calculation with a generalized-gradient approximation functional including spin-orbit coupling (SOC). The cut-off energy of plane wave basis and the conversion criterion are adopted 50 Ry and 10^{-8} Ry, respectively.

	x	y	z
Co ⁽¹⁾	0.144	0.144	0.144
Co ⁽²⁾	0.644	0.356	0.856
Co ⁽³⁾	0.356	0.856	0.644
Co ⁽⁴⁾	0.856	0.644	0.356
Se ⁽¹⁾	0.843	0.843	0.843
Se ⁽²⁾	0.343	0.657	0.157
Se ⁽³⁾	0.657	0.157	0.343
Se ⁽⁴⁾	0.157	0.343	0.657

TABLE I. The list of atomic positions in the unit cell of CoSi, which is shown in Fig. 1(a). The positions are represented in units of the lattice constant.

In the band structure of Fig. 1(c), nodes appear at two high-symmetry points. At the Γ point, electronic states

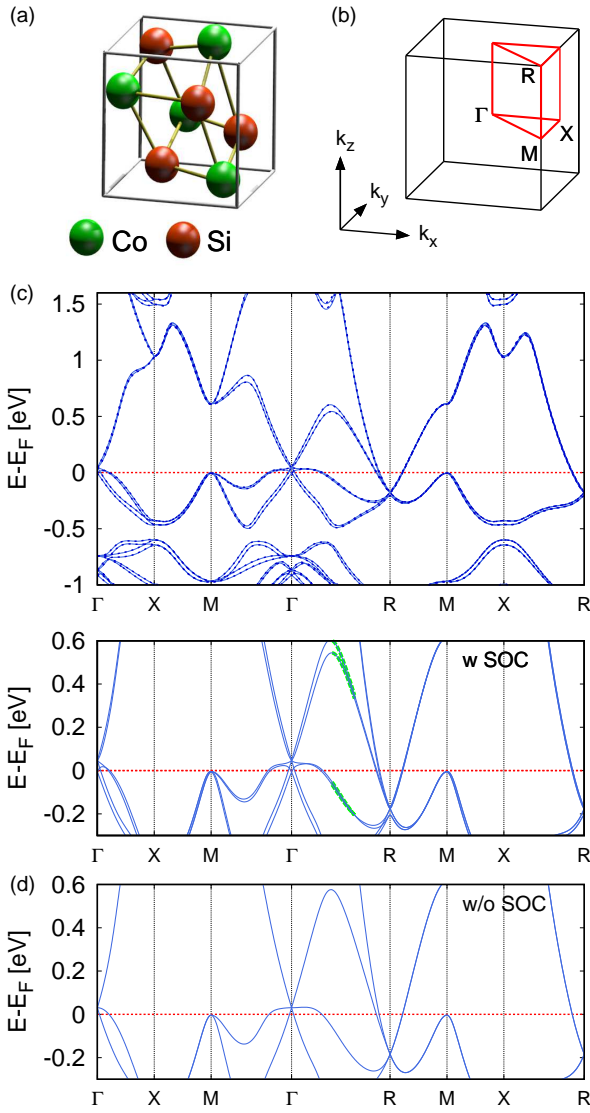


FIG. 1. The unit cell and the Brillouin zone for CoSi in (a) and (b), respectively. The band structure of CoSi calculated by first-principles calculation including the spin-orbit coupling in (c). The band within different energy ranges is depicted in the upper and lower panels. The dashed line in the upper panel indicates the band calculated by the tight-binding model discussed in Sec. III. In (d), the band is calculated without the spin-orbit interaction.

are quadruply degenerated at the upper node and doubly degenerated at the lower node, where these nodes are split due to SOC¹⁷. The four-fold degenerated node is slightly above the Fermi level, and a doubly degenerate node emerges just below the level. In the absence of SOC, these nodes are degenerate as shown in Fig. 1(d). The node at the *R* point appears with sextuple degeneration 175meV below the Fermi energy. At the *R* point, four cones and a single spin-split band are crossing, and two hole bands split due to SOC. The local maximum of valence band emerges at the *M* point with a gap of

620meV.

III. DYNAMICAL CONDUCTIVITY

The dynamical conductivity $\sigma(\omega)$ is associated with the optical property. The real part $\sigma_1(\omega) = \text{Re}[\sigma(\omega)]$ is proportional to the optical absorption, and the photon-energy dependence shows the unique spectrum due to the electronic structure of nodal semimetal^{14,15,18–27}. We represent the electronic states in CoSi by using a multi-orbital tight-binding model in the basis of Wannier functions. We adopt five *d*-orbitals in Co and three *p*-orbitals in Se as the basis of Wannier function and compute the spin-dependent hopping integrals from the first-principle bands in Fig. 1 by using Wannier90, a code for calculating maximally localized Wannier function and the hopping matrix²⁸. This tight-binding model reproduces the band structure as shown in Fig. 1.

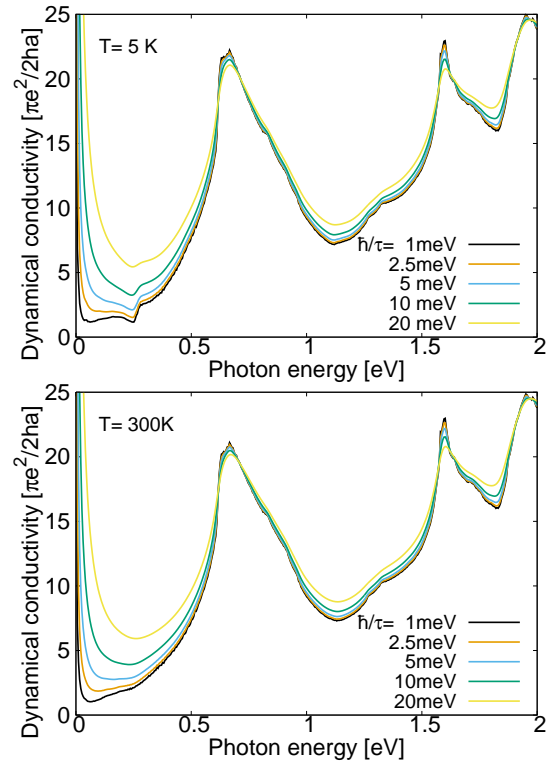


FIG. 2. The dynamical conductivity as a function of photon energy is plotted for several relaxation-time, $\hbar/\tau = 1, 2.5, 5, 10,$ and 20 meV, at 5K and 300K.

We calculate the dynamical conductivity in the linear response theory where it for a linearly polarizing photon is represented by

$$\sigma(\omega, T) = \frac{2i e^2}{\omega \hbar} \sum_{m \leq n} \int_{\text{BZ}} \frac{d^3 \mathbf{k}}{(2\pi)^3} \frac{|\langle n\mathbf{k} | \hat{v}_\alpha | m\mathbf{k} \rangle|^2}{\omega - (E_{n\mathbf{k}} - E_{m\mathbf{k}}) + i\hbar/(2\tau)} \times (n_F(E_{\alpha\mathbf{k}}, T) - n_F(E_{\beta\mathbf{k}}, T)), \quad (1)$$

where $n_F(E, T)$ is Fermi distribution function at the temperature T and the energy E with respect to the Fermi level. Here, ω is the frequency of photon, and the velocity is defined by the commutation of the position and the Hamiltonian, $\hat{v}_\alpha = (1/i\hbar)[x_\alpha, H]$, where α is parallel to the polarizing direction of photon. The eigenstate $|m\mathbf{k}\rangle$ and the energy $E_{m\mathbf{k}}$ are calculated by using the multi-orbital tight-binding Hamiltonian. The effect of impurity is included in Eq. 1 as the relaxation time τ .

We consider the dynamical conductivity for linearly-polarized photons in (100) direction and show the relaxation time-dependence of $\sigma_1(\omega)$ at $T = 5\text{K}$ and 300K in Fig. 2. The low-frequency spectrum is sensitive to τ in $\omega < 500\text{meV}$ because of the Drude peak, an intra-band excitation existing around $\omega = 0$. Since the Drude peak narrows with increase in the relaxation time, the inter-band excitation can be visible even in the low-frequency region. In this region, the spectrum reflects the excitation between electronic states around nodes in the Brillouin zone. In the ballistic condition, $\hbar/\tau = 1\text{meV}$, the dynamical conductivity linearly increases with ω up to $\omega \sim 150\text{meV}$ at both the temperatures. The linear dependence is a characteristic feature of three-dimensional point-nodal semimetals.^{23,29} This characteristic spectrum disappears with a decrease of τ , i.e., an increase of disorder, due to the broadening of Drude peak but it is stable in a clean sample even at the room temperature. In Fig. 3, we show the temperature dependence of $\sigma_1(\omega)$ up to the room temperature. It exhibits that the linear slope is unchanged with increase in temperature. In what follows, we investigate the relation between electronic states of the topological semimetal and characteristic features in the spectrum of $\sigma_1(\omega)$.

Firstly, we find that a dip structure emerges around $\omega \sim 250\text{meV}$ in the spectrum of $\sigma_1(\omega)$ below 200K . This structure looks similar to one in a recent work²⁹ but the origin is not same. The temperature dependence means that the electronic states near the Fermi level are associated to the dip structure. A sharp step of upper slope is consistent with the spectrum of a partially-filled Dirac cone, where the step-like structure emerges due to the excitation of electrons near the Fermi level.³⁰ At the R point, the cone is partially filled, and the frequency of the step agrees with the excitation energy to electronic states in the Fermi level from the lower band. Thus, the step indicates that the spectrum above the step includes electronic excitation in the Dirac cone at the R point. Moreover, the sharp structure is attributed to the isotropic excitation energy for electronic states in the Fermi pocket around the node.

Below the dip, on the other hand, $\sigma_1(\omega)$ smoothly decreases without the step structure. The downward slop is attributed to the middle band, a band between the upper cone and the lower cone at the Γ point, crossing over the Fermi level near the node. In the Γ - R axis, the three-fold rotation axis, the excitation between the upper and lower cones is inhibited as discussed later. Thus, the drop of middle band across the Fermi energy changes the exci-

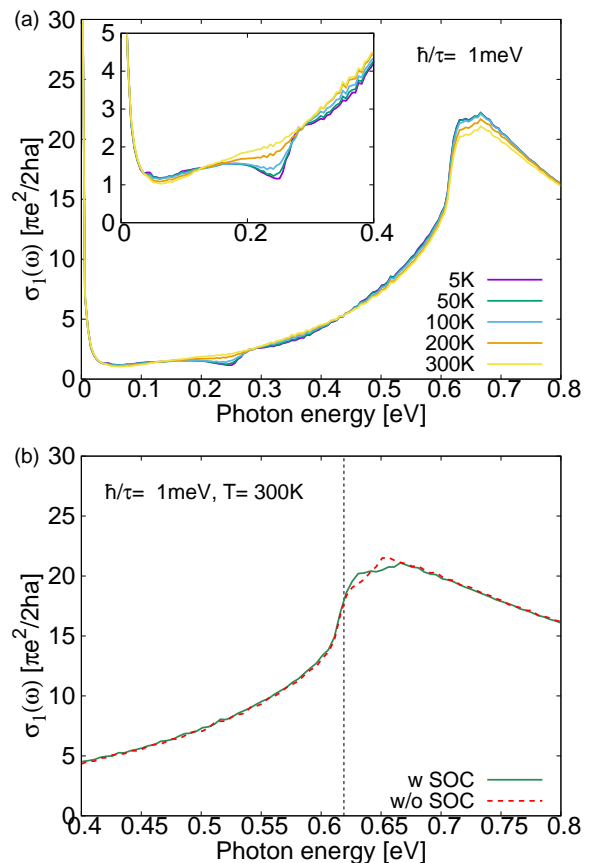


FIG. 3. The dynamical conductivity plotted at several temperatures, $T = 5, 10, 50, 100,$ and 300K , for $\hbar/\tau = 1\text{meV}$ and 10meV in (a). In (b), the dynamical conductivity calculated with and without the spin-orbit coupling. The dashed line indicates the minimal excitation energy at the M point.

tation from (1) the lower cone-middle band excitation to (2) the middle band-upper cone excitation in $\sigma_1(\omega)$. The excitation energy of (1) is larger than that of (2) near the crossover point due to the drop of middle band. Thus, the decline of $\sigma_1(\omega)$ due to the disappearance of (1) is not covered by (2) around 200meV . The inhibition of excitation between the upper and lower cones is a characteristic feature of the multi-fold chiral fermionic states different from the conventional Dirac fermionic states, where the inter-cone excitation is responsible for the dynamical conductivity¹⁸.

We discuss the inhibition of excitation between cones. This feature is a characteristic of the chiral fermionic states at the Γ point. To analyze the inhibition, we consider the amplitude of atomic orbitals in electronic states. The three bands, the upper and lower cones, and the middle band, mainly consist of d -orbitals in four Co atoms. We show the amplitude of these orbitals in Fig. 4 where the amplitude is represented by the size of mark for each d -orbital with the magnetic angular momentum m and the spin is indicated by the color. The main components

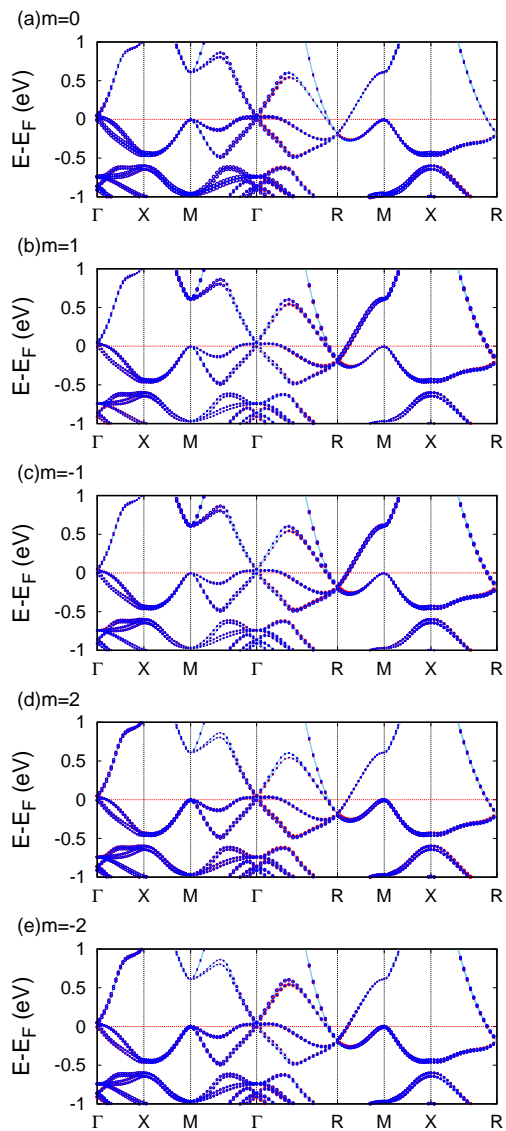


FIG. 4. The amplitude of d -orbitals in electronic states. The d -orbitals with an magnetic angular momentum $m = 0, \pm 1$, and ± 2 along the (001) direction are considered in Co. The marks represent the amplitude by the size and the spin by the color, where the up-spin and the down-spin are represented by red and blue, respectively.

of the three bands are $m = 0$ and $m = \pm 2$ orbitals. Thus, the excitation between the different orbitals is absent due to the selection rule, which allows the excitation with the change of magnetic angular momentum $\Delta m = 0$ only for $m \neq 0$ orbital and ± 1 for all orbitals. In Γ - R direction, the excitation between the upper and lower cones is inhibited because the $m = -2$ ($m = 2$) orbital has the amplitude in the middle and upper(lower) cone, and the amplitude of $m = 0$ orbital distributes in three bands. Therefore, the dip structure exhibits the characteristics of both the band structure and the electronic states of the multi-fold chiral fermion. This dip also shows the

exchange of the dominant electronic states in $\sigma_1(\omega)$ from the chiral fermion in the Γ point to that in the R point.

Secondly, we focus on a peak with a flat top around $\omega \simeq 650\text{meV}$. This flat-top peak exhibits the effect of SOC to the nodal band structure around the R point. In the practice, the peak structure changes with the presence of SOC as shown in Fig. 3(b). It is not ascribable to a simple excitation between the local minimum of conduction band and maximum of valence band. The excitation energy at the M point, the vertical dashed line in Fig. 3(b), is close to the peak energy but it is slightly smaller than the peak energy and the electronic states does not split even in the presence of SOC. The numerical calculation can reveal the electronic states which are responsible to $\sigma_1(\omega)$ by computing the integrand in Eq. 1. We show the electronic states associated with the excitation corresponding to the flat-top peak by shading in Fig. 1(c). The occupied and unoccupied states are distributed in the aligned lines, where the unoccupied band splits into two by SOC. The density of states with the same excitation energy is enhanced in the case of aligned lines as a case about the nodal-line semimetal¹⁴, and the enhancement emerges in $\sigma_1(\omega)$ around the energy as a peak. Since the split due to SOC gradually decreases to the R point, the excitation energy is distributed in a range corresponding to the SOC split and it produces a flat-top peak consisting of a series of peaks with energy continuously changing. Therefore, the flat-top peak exhibits the SOC split in the band of multi-fold chiral fermion at the R point.

Finally, in higher-frequency region, we find the other peaks at $\omega \simeq 1.6\text{ eV}$ and 1.9 eV . The two peaks are attributed to the local maximum and minimum of energy dispersion at high symmetry points. The peak at 1.6 eV is corresponding to the excitation between the lowest conduction band and the second highest valence band around -1 eV at the M point. The another peak emerges at 1.9 eV due to the excitation between the highest valence band and the band slightly above 1.5 eV at the X point. The spectrum in a higher energy region reflects higher-energy conduction and lower-energy valence bands.

IV. CONCLUSION

We have investigated the dynamical conductivity of CoSi, a novel topological semimetal holding multi-fold chiral fermion, by using first-principle band calculation and linear response theory. The spectrum of dynamical conductivity $\sigma_1(\omega)$ exhibits dip and peak structures at some photon frequency ω associated with the characteristic electronic structure. We have found three characteristic features associated with the multi-fold chiral fermions in the spectrum. Firstly, in the low-frequency $\omega < 150\text{meV}$, the dynamical conductivity behaves as a linear function of frequency. This is attributed to the linear band dispersion around the node at the Γ point. Sec-

ondary, unlike Dirac and Weyl semimetals, the dynamical conductivity decreases from $\omega = 150\text{eV}$ and forms a dip structure around $\omega = 200\text{meV}$. This dip structure is attributed to the electronic states of the chiral fermion. Finally, a peak structure at $\omega = 650\text{meV}$ re-

flects the dispersion of chiral fermion at the R point and has a flat-top due to the split by SOC. These features can be fingerprints corresponding to electronic states of the novel point-nodal semimetal in the experiment.

-
- ¹ S. Murakami, *New Journal of Physics* **9**, 356 (2007).
- ² X. Wan, A. M. Turner, A. Vishwanath, and S. Y. Savrasov, *Phys. Rev. B* **83**, 205101 (2011).
- ³ K.-Y. Yang, Y.-M. Lu, and Y. Ran, *Phys. Rev. B* **84**, 075129 (2011).
- ⁴ A. A. Burkov and L. Balents, *Phys. Rev. Lett.* **107**, 127205 (2011).
- ⁵ M. Neupane, S. Xu, R. Sankar, N. Alidoust, G. Bian, C. Liu, I. Belopolski, T.-R. Chang, H.-T. Jeng, H. Lin, A. Bansil, F. Chou, and M. Z. Hasan, *Nature Communications* **5**, 3786 (2014).
- ⁶ S. Borisenko, Q. Gibson, D. Evtushinsky, V. Zabolotnyy, B. Büchner, and R. J. Cava, *Phys. Rev. Lett.* **113**, 027603 (2014).
- ⁷ B. Bradlyn, L. Elcoro, J. Cano, M. G. Vergniory, Z. Wang, C. Felser, M. I. Aroyo, and B. A. Bernevig, *Nature* **547**, 298 (2017).
- ⁸ P. Tang, Q. Zhou, and S.-C. Zhang, *Phys. Rev. Lett.* **119**, 206402 (2017).
- ⁹ B. Bradlyn, L. Elcoro, M. G. Vergniory, J. Cano, Z. Wang, C. Felser, M. I. Aroyo, and B. A. Bernevig, *Phys. Rev. B* **97**, 035138 (2018).
- ¹⁰ P. Dutta and S. K. Pandey, *Computational Condensed Matter* **16**, e00325 (2018).
- ¹¹ D. A. Pshenay-Severin, Y. V. Ivanov, and A. T. Burkov, *Journal of Physics: Condensed Matter* **30**, 475501 (2018).
- ¹² D. Takane, Z. Wang, S. Souma, K. Nakayama, T. Nakamura, H. Oinuma, Y. Nakata, H. Iwasawa, C. Cacho, T. Kim, K. Horiba, H. Kumigashira, T. Takahashi, Y. Ando, and T. Sato, *Phys. Rev. Lett.* **122**, 076402 (2019).
- ¹³ Z.-C. Rao, H. Li, T.-T. Zhang, S.-J. Tian, C.-H. Li, B.-B. Fu, C.-Y. Tang, L. Wang, Z.-L. Li, W.-H. Fan, *et al.*, arXiv preprint arXiv:1901.03358 (2019).
- ¹⁴ T. Habe and M. Koshino, *Phys. Rev. B* **98**, 125201 (2018).
- ¹⁵ M. B. Schilling, L. M. Schoop, B. V. Lotsch, M. Dressel, and A. V. Pronin, *Phys. Rev. Lett.* **119**, 187401 (2017).
- ¹⁶ P. Giannozzi, S. Baroni, N. Bonini, M. Calandra, R. Car, C. Cavazzoni, D. Ceresoli, G. L. Chiarotti, M. Cococcioni, I. Dabo, A. Dal Corso, S. de Gironcoli, S. Fabris, G. Fratesi, R. Gebauer, U. Gerstmann, C. Gougousis, A. Kokalj, M. Lazzeri, L. Martin-Samos, N. Marzari, F. Mauri, R. Mazzarello, S. Paolini, A. Pasquarello, L. Paulatto, C. Sbraccia, S. Scandolo, G. Sclauzero, A. P. Seitsonen, A. Smogunov, P. Umari, and R. M. Wentzcovitch, *J. Phys.: Condens. Matter* **21**, 395502 (2009).
- ¹⁷ F. Ishii, H. Kotaka, and T. Onishi, “Spinorbit interaction effects in the electronic structure of b20-type cosi: First-principles density functional study,” in *Proceedings of the International Conference on Strongly Correlated Electrons* (2014) <https://journals.jps.jp/doi/pdf/10.7566/JPSCP.3.016019>.
- ¹⁸ T. Ando, Y. Zheng, and H. Suzuura, *Journal of the Physical Society of Japan* **71**, 1318 (2002).
- ¹⁹ V. P. Gusynin and S. G. Sharapov, *Phys. Rev. B* **73**, 245411 (2006).
- ²⁰ M. Koshino and T. Ando, *Phys. Rev. B* **77**, 115313 (2008).
- ²¹ T. Stauber, N. M. R. Peres, and A. K. Geim, *Phys. Rev. B* **78**, 085432 (2008).
- ²² K. F. Mak, M. Y. Sfeir, Y. Wu, C. H. Lui, J. A. Misewich, and T. F. Heinz, *Phys. Rev. Lett.* **101**, 196405 (2008).
- ²³ C. J. Tabert and J. P. Carbotte, *Phys. Rev. B* **93**, 085442 (2016).
- ²⁴ S. P. Mukherjee and J. P. Carbotte, *Phys. Rev. B* **95**, 214203 (2017).
- ²⁵ S. Ahn, E. J. Mele, and H. Min, *Phys. Rev. Lett.* **119**, 147402 (2017).
- ²⁶ S. Barati and S. H. Abedinpour, *Phys. Rev. B* **96**, 155150 (2017).
- ²⁷ J. Ebad-Allah, J. F. Afonso, M. Krottenmüller, J. Hu, Y. Zhu, Z. Mao, J. Kuneš, and C. Kuntscher, arXiv preprint arXiv:1901.10256 (2019).
- ²⁸ A. A. Mostofi, J. R. Yates, Y.-S. Lee, I. Souza, D. Vanderbilt, and N. Marzari, *Computer Physics Communications* **178**, 685 (2008).
- ²⁹ M.-Á. Sánchez-Martínez, F. de Juan, and A. G. Grushin, arXiv preprint arXiv:1902.07271 (2019).
- ³⁰ S. P. Mukherjee and J. P. Carbotte, *Journal of Physics: Condensed Matter* **29**, 425301 (2017).